Journal of Solid State Chemistry 183 (2010) 1504–1509

Contents lists available at ScienceDirect

Journal of Solid State Chemistry

journal homepage: www.elsevier.com/locate/jssc

Thermal decomposition behavior of the rare-earth ammonium sulfate $R_2(SO_4)_3 \cdot (NH_4)_2SO_4$

Tsukasa Nagai [a,b], Shinji Tamura [a], Nobuhito Imanaka [a,*]

[a] Department of Applied Chemistry, Faculty of Engineering, Osaka University, 2-1 Yamadaoka, Suita, Osaka 565-0871, Japan
[b] Japan Society for the Promotion of Science, 1-8 Chiyoda-ku, Tokyo 102-8472, Japan

ARTICLE INFO

Article history:
Received 23 January 2010
Received in revised form
22 April 2010
Accepted 25 April 2010
Available online 13 May 2010

Keywords:
Rare-earth ammonium sulfate
Ammonium sulfate
Rare-earth sulfate
Raman
Infrared

ABSTRACT

Rare-earth ammonium sulfate octahydrates of $R_2(SO_4)_3 \cdot (NH_4)_2SO_4 \cdot 8H_2O$ (R=Pr, Nd, Sm, and Eu) were synthesized by a wet process, and the stable temperature region for the anhydrous $R_2(SO_4)_3 \cdot (NH_4)_2SO_4$ form was clarified by thermogravimetry/differential thermal analysis, infrared, Raman, and electrical conductivity measurements. Detailed characterization of these double salts demonstrated that the thermal stability of anhydrous $R_2(SO_4)_3 \cdot (NH_4)_2SO_4$ is different between the Pr, Nd salts and the Sm, Eu salts, and the thermal decomposition behavior of these salts was quite different from the previous reports.

1. Introduction

In general, the physical properties of ammonium salts are similar to those of potassium and rubidium salts in terms of crystalline structure, molar volume, and solubility in water, because the ionic radius of the ammonium ion is close to that of potassium and rubidium ion. However, since the thermal stability of ammonium salts is significantly lower than that of these alkali metal salts, many ammonium salts decompose and ammonium ions in solids vaporize below 200 °C. In contrast, the double sulfate salts formed by ammonium ions (NH_4^+) and trivalent metal ions (M^{3+}), which are generally described as $M_2(SO_4)_3 \cdot (NH_4)_2SO_4$, have a high thermal stability compared to other ammonium salts, and the decomposition temperature of $M_2(SO_4)_3 \cdot (NH_4)_2SO_4$ salts is between 300 and 400 °C [1–7].

Double sulfates such as ammonium alum and iron alum are generally obtained as the hydrate form of $M_2(SO_4)_3 \cdot (NH_4)_2SO_4 \cdot xH_2O$ (x=2–12). Although the anhydrate form of these salts, called burnt ammonium alum ($M_2(SO_4)_3 \cdot (NH_4)_2SO_4$), can be obtained by vaporizing the crystallization water by the heat treatment above 300 °C, it is difficult to obtain the solid state form because of the low melting point ($\leq$100 °C) of $M_2(SO_4)_3 \cdot (NH_4)_2SO_4 \cdot xH_2O$ solids. Among these double sulfates containing ammonium ions, rare-earth ammonium sulfates, $R_2(SO_4)_3 \cdot (NH_4)_2SO_4 \cdot xH_2O$ (R=rare-earth, x=2–8; this series can be presented to be $(NH_4)[R(SO_4)_2(H_2O)_3] \cdot (H_2O)$ as a general metal complex presentation), are interesting materials in that they have no melting point and form the anhydrate at low temperatures [8,9]. While many investigations of their chemical or physical properties have been carried out [10–13], the thermal behavior of $R_2(SO_4)_3 \cdot (NH_4)_2SO_4 \cdot xH_2O$ was studied only by thermogravimetry/differential thermal analysis (TG-DTA).

In our previous work on a solid electrolyte type NH_3 gas sensor [14,15], we found that the sensor with rare-earth ammonium sulfate of anhydrous $R_2(SO_4)_3 \cdot (NH_4)_2SO_4$ (R=Pr, Nd), as the auxiliary sensing electrode had excellent NH_3 gas sensing performance at 230 °C, where the crystallization water in $R_2(SO_4)_3 \cdot (NH_4)_2SO_4 \cdot xH_2O$ fully vaporized with no decomposition of the $R_2(SO_4)_3 \cdot (NH_4)_2SO_4$ solid. In this work, we found that the thermal stability of the $R_2(SO_4)_3 \cdot (NH_4)_2SO_4$ solids (R=Pr, Nd) differed from the values reported in the literature [9].

In this study, we clarified the stable temperature region for $R_2(SO_4)_3 \cdot (NH_4)_2SO_4$ solids (R=Pr, Nd, Sm, Eu), which were obtained from mixed aqueous solutions of equimolar amounts of rare-earth sulfate and ammonium sulfate, by TG-DTA, IR, and Raman analyses and electrical conductivity measurements.

2. Experimental

2.1. Preparation of rare-earth ammonium sulfate $R_2(SO_4)_3 \cdot (NH_4)_2SO_4$

Rare-earth ammonium sulfate double salts of $R_2(SO_4)_3 \cdot (NH_4)_2SO_4$ (R=Pr, Nd, Sm, Eu, Gd, Tb, Ho, Yb, Lu) were synthesized by a

* Corresponding author. Fax: +81 6 6879 7354.
E-mail address: imanaka@chem.eng.osaka-u.ac.jp (N. Imanaka).

0022-4596/$ - see front matter © 2010 Elsevier Inc. All rights reserved.
doi:10.1016/j.jssc.2010.04.038

wet process. Each rare-earth oxide was dissolved in 3 mol l^{-1} HCl solution at 100 °C, and then concentrated H_2SO_4 (98%) was added into the HCl solution, in the proportion of 1 mol R^{3+} ion to 1.5 mol of SO_4^{2-} ion, to produce $R_2(SO_4)_3$. After cooling the solution to room temperature, $R_2(SO_4)_3$ precipitates were obtained by adding an excess amount of ethanol. The precipitate was washed with ethanol until both H^+ and Cl^- ions were rinsed off. The $R_2(SO_4)_3$ obtained was dried, and mixed with an equimolar amount of $(NH_4)_2SO_4$, and then dissolved in water. By heating the solution at 60–100 °C to vaporize the water, $R_2(SO_4)_3 \cdot (NH_4)_2SO_4 \cdot xH_2O$ was obtained.

2.2. Experimental techniques

X-ray powder diffraction patterns of the samples were obtained at room temperature using Ni filtered Cu-$K\alpha$ radiation (λ=1.54178 Å) in the 2θ range from 10° to 30° with steps of 2° or 0.02° (Multiflex, Rigaku). Thermal analysis (Thermogravimetric, TG and differential thermal analysis, DTA) was carried out (DTA-60H, Shimadzu) in a synthetic air atmosphere. The heating rates were 2 and 10 °C min^{-1} for TG and DTA, respectively. A platinum crucible was used as a container and alumina was used as a reference material for DTA measurements. Infrared spectra were measured for the $R_2(SO_4)_3 \cdot (NH_4)_2SO_4 \cdot xH_2O$ (R=Pr, Nd, Sm, Eu) solids, which were obtained by heating the $R_2(SO_4)_3 \cdot (NH_4)_2SO_4 \cdot 8H_2O$ powder at 120–260 °C for 10 h in air in the 4000–400 cm^{-1} region (FT/IR-430, Jasco) by mixing dry KBr. Raman spectra in the range of 1200–200 cm^{-1} were investigated using a 532 nm laser as an excitation source (NRS-3100 spectrometer, Jasco). The sample powder of $R_2(SO_4)_3 \cdot (NH_4)_2SO_4$ (R=Pr, Nd, Sm, Eu) for Raman analysis was obtained by heating the $R_2(SO_4)_3 \cdot (NH_4)_2SO_4 \cdot 8H_2O$ powder at 220–340 °C for 10 h in air.

Electrical conductivity of the anhydrous $R_2(SO_4)_3 \cdot (NH_4)_2SO_4$ (R=Pr, Nd, Sm, Eu) solids was measured by a complex impedance method at frequency of 5–13 MHz (Precision LCR meter 8284A, Hewlett Packard) at temperatures ranging from 50 to 350 °C. The anhydrate $Pr_2(SO_4)_3 \cdot (NH_4)_2SO_4$ powder was obtained by heating $R_2(SO_4)_3 \cdot (NH_4)_2SO_4 \cdot 8H_2O$ powder at 200 °C for 10 h in air. The resulting anhydrous $R_2(SO_4)_3 \cdot (NH_4)_2SO_4$ was formed into pellets and sintered at 200 °C (R=Pr, Nd) or 240 °C (R=Sm, Eu), for 10 h in air.

3. Results and discussion

3.1. Synthesis of $R_2(SO_4)_3 \cdot (NH_4)_2SO_4 \cdot xH_2O$

Fig. 1 depicts X-ray powder diffraction patterns (XRD) of the samples obtained from equimolar amounts of $R_2(SO_4)_3$ (R=Pr, Nd, Sm, Eu, Gd, Tb, Ho, Yb, Lu) and $(NH_4)_2SO_4$. The structure of $R_2(SO_4)_3 \cdot (NH_4)_2SO_4 \cdot 8H_2O$, whose space group of $P21/c$ ($Nd_2(SO_4)_3 \cdot (NH_4)_2SO_4 \cdot 8H_2O$: PDF #000-009-0283) was reported in the literature [10], is also shown. XRD measurements of these samples indicated that a single phase of $R_2(SO_4)_3 \cdot (NH_4)_2SO_4 \cdot 8H_2O$ was obtained from the R=Pr, Nd, Sm, and Eu samples. The X-ray powder data for the $R_2(SO_4)_3 \cdot (NH_4)_2SO_4 \cdot xH_2O$ (R=Pr, Nd, Sm, Eu) solids are summarized in Table 1. The diffraction peaks of the $R_2(SO_4)_3 \cdot (NH_4)_2SO_4 \cdot 8H_2O$ phase shifted to higher angles with increasing atomic number of rare-earth elements because of the

Table 1
X-ray powder data for $R_2(SO_4)_3 \cdot (NH_4)_2SO_4 \cdot 8H_2O$ (R=Pr, Nd, Sm, Eu).

	Pr		Nd		Sm		Eu	
$h\,k\,l$	d (Å)	I/I_0	d (Å)	I/I_0	d (Å)	I/I_0	d (Å)	I/I_0
0 1 1	7.8939	0.9	7.8376	1.6	7.8512	1.2	7.8885	1.6
1 0 0	6.5725	21.6	6.5158	28.2	6.4959	19.1	6.5058	33.4
0 2 1	6.3932	100.0	6.3653	100.0	6.3571	100.0	6.3752	100.0
1 1 0	6.2066	15.6	6.1636	26.7	6.1462	15.2	6.1551	30.4
−1 2 0	5.3950	2.6	5.3680	4.5	5.3547	2.7	5.3554	5.8
−1 2 1	4.8080	7.3	4.7864	10.5	4.7662	7.4	4.7712	17.9
0 4 0	4.7260	40.9	4.7057	74.3	4.7012	21.6	4.7114	21.8
0 0 2	4.3540	21.4	4.3369	21.5	4.3283	12.1	4.3291	20.6
0 1 2	4.2394	9.4	4.2231	12.9	4.2184	8.8	4.2190	14.9
−1 3 1	4.1566	7.3	4.1484	10.7	4.1374	7.2	4.1449	16.3
0 2 2	3.9522	4.4	3.9409	4.6	–	–	3.9345	4.8
−1 4 0	3.8504	2.9	3.8307	3.4	–	–	3.8208	6.3
−1 2 2	3.5784	1.1	3.5587	1.7	3.5422	1.0	3.5372	2.3
1 0 2	3.4791	3.6	3.4556	2.8	3.4551	1.5	3.4579	2.6
1 1 2	3.3860	2.4	3.3709	3.6	3.3637	1.8	3.3703	4.9
−1 3 2	3.2899	9.9	3.2713	11.4	3.2594	6.5	3.2615	16.6
−2 1 0	3.2452	20.8	3.2291	17.0	3.2131	14.6	3.2088	28.0
0 4 2	3.2043	21.0	3.1889	43.9	3.1883	21.5	–	–
0 6 0	3.1554	14.9	3.1445	27.9	3.1358	10.2	3.1336	13.9

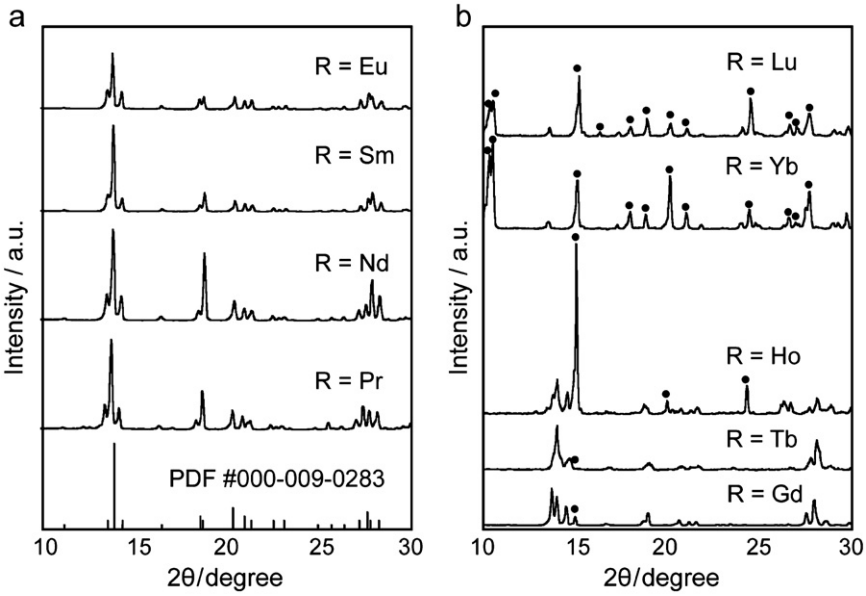

Fig. 1. X-ray powder diffraction patterns of the sample obtained from an equimolar mixture of $R_2(SO_4)_3$ and $(NH_4)_2SO_4$ (R=Pr, Nd, Sm, Eu, Gd, Tb, Ho, Yb, Lu). The closed circles (●) represent the diffraction peak of the rare-earth sulfate hydrate of $R_2(SO_4)_3 \cdot nH_2O$.

lanthanide contraction. On the other hand, a secondary phase of $R_2(SO_4)_3 \cdot xH_2O$ ($x=3$–8) was observed in addition to $R_2(SO_4)_3 \cdot (NH_4)_2SO_4 \cdot 8H_2O$ for R=Gd, Tb, and Ho samples. Moreover, for R=Yb and Lu, the main phase of the compounds was $R_2(SO_4)_3 \cdot xH_2O$, although the $R_2(SO_4)_3 \cdot (NH_4)_2SO_4 \cdot 8H_2O$ phase also appeared. Therefore, the single phase of the $R_2(SO_4)_3 \cdot (NH_4)_2SO_4 \cdot xH_2O$ double salt could be obtained only for Pr, Nd, Sm, and Eu from an equimolar mixture of $R_2(SO_4)_3$ and $(NH_4)_2SO_4$, which agrees with the previous report [9] that $R_2(SO_4)_3 \cdot (NH_4)_2SO_4 \cdot xH_2O$ can be obtained for R=Pr, Nd, Sm, and Eu.

3.2. Thermal analysis of $R_2(SO_4)_3 \cdot (NH_4)_2SO_4 \cdot 8H_2O$ (R=Pr, Nd, Sm, and Eu)

To investigate the stable temperature region for anhydrous $R_2(SO_4)_3 \cdot (NH_4)_2SO_4$, thermogravimetric analysis (TG) and differential thermal analysis (DTA) were measured with heating rates of 2 and 10 °C min^{-1} respectively. Fig. 2 shows the thermal analysis results for (a) $Pr_2(SO_4)_3 \cdot (NH_4)_2SO_4 \cdot 8H_2O$ and (b) $Sm_2(SO_4)_3 \cdot (NH_4)_2SO_4 \cdot 8H_2O$ solids. Table 2 summarizes the detailed TG-DTA results for $R_2(SO_4)_3 \cdot (NH_4)_2SO_4 \cdot 8H_2O$ (R=Pr, Nd, Sm, and Eu). Although the weight lost, which suggested the dehydration of crystallization water, corresponded well with the theoretical estimates based on the stoichiometry of $R_2(SO_4)_3 \cdot (NH_4)_2SO_4 \cdot 8H_2O$ (16–17%), the dehydration nature of $R_2(SO_4)_3 \cdot (NH_4)_2SO_4 \cdot 8H_2O$ salt was found to be markedly different between the Pr, Nd salts and the Sm, Eu salts. For $Pr_2(SO_4)_3 \cdot (NH_4)_2SO_4 \cdot 8H_2O$ and $Nd_2(SO_4)_3 \cdot (NH_4)_2SO_4 \cdot 8H_2O$ solids (Fig. 2a), a two-step weight loss (ca. 17%; the first weight loss was ca. 13% and second one was ca. 4%) accompanied by large endothermic peaks, which coincides well with the total amount of crystallization water, $8H_2O$ (ca. 17%), was clearly observed at temperatures between 75 and 180 °C. Therefore, the dehydration process of $R_2(SO_4)_3 \cdot (NH_4)_2SO_4 \cdot 8H_2O$ (R=Pr, Nd) compounds can be presented as

$$R_2(SO_4)_3 \cdot (NH_4)_2SO_4 \cdot 8H_2O \rightarrow R_2(SO_4)_3 \cdot (NH_4)_2SO_4 \cdot 2H_2O + 6H_2O\uparrow, \quad (1)$$

$$R_2(SO_4)_3 \cdot (NH_4)_2SO_4 \cdot 2H_2O \rightarrow R_2(SO_4)_3 \cdot (NH_4)_2SO_4 + 2H_2O\uparrow. \quad (2)$$

In contrast, the $Sm_2(SO_4)_3 \cdot (NH_4)_2SO_4 \cdot 8H_2O$ and $Eu_2(SO_4)_3 \cdot (NH_4)_2SO_4 \cdot 8H_2O$ solids (Fig. 2b) have a two-step weight loss (ca. 15%) with large endothermic peaks, the amount corresponds to seven water molecules at temperatures of 80–140 °C, and gradual weight loss corresponding to one water molecule (ca. 2%) was observed between

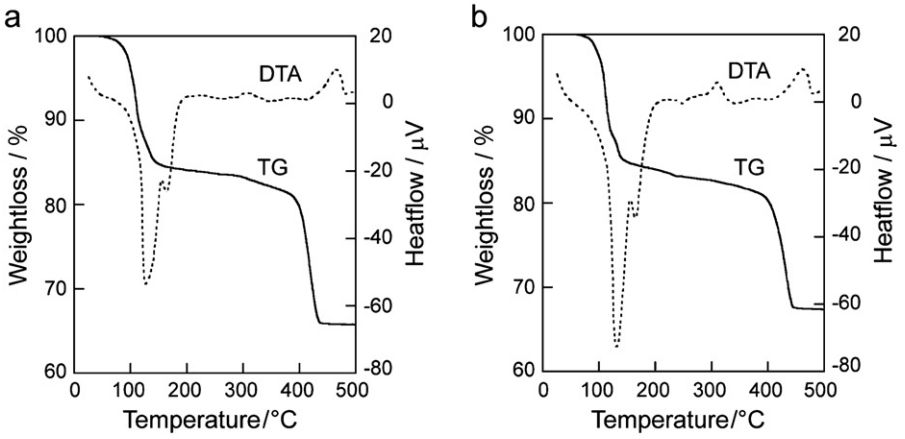

Fig. 2. TG-DTA results of the $R_2(SO_4)_3 \cdot (NH_4)_2SO_4 \cdot 8H_2O$ solids: (a) R=Pr and (b) R=Sm.

Table 2
TG-DTA results of $R_2(SO_4)_3 \cdot (NH_4)_2SO_4 \cdot 8H_2O$ (R=Pr, Nd, Sm, Eu).

R	Temperature (°C)	Measurement		Theoretical	
		Weight loss (%)	Number of moles	Weight loss (%)	Number of moles
Pr	75.0–146.0	13.1	$6H_2O$	12.8	$6H_2O$
	146.0–175.0	4.6	$2H_2O$	4.3	$2H_2O$
	301.3 (+)	–	–	–	–
	272.0–475.0	16.4	1 $(NH_4)_2SO_4$	15.6	1 $(NH_4)_2SO_4$
Nd	79.0–151.5	12.8	$6H_2O$	12.7	$6H_2O$
	151.5–179.0	4.1	$2H_2O$	4.2	$2H_2O$
	308.2 (+)	–	–	–	–
	274.5–478.5	16.7	1 $(NH_4)_2SO_4$	15.5	1 $(NH_4)_2SO_4$
Sm	79.8–126.5	12.3	$6H_2O$	12.5	$6H_2O$
	126.5–140.5	2.3	$1H_2O$	2.1	$1H_2O$
	140.5–240.5	2.2	$1H_2O$	2.1	$1H_2O$
	310.4 (+)	–	–	–	–
	290.5–447.5	15.6	1 $(NH_4)_2SO_4$	15.3	1 $(NH_4)_2SO_4$
Eu	83.5–120.4	12.4	$6H_2O$	12.5	$6H_2O$
	120.4–135.3	2.4	$1H_2O$	2.1	$1H_2O$
	135.3–235.5	2.1	$1H_2O$	2.1	$1H_2O$
	313.1 (+)	–	–	–	–
	292.5–448.5	16.3	1 $(NH_4)_2SO_4$	15.2	1 $(NH_4)_2SO_4$

140 and 240 °C. Therefore, the dehydration behavior of $R_2(SO_4)_3 \cdot (NH_4)_2SO_4 \cdot 8H_2O$ (R=Sm, Eu) compounds is found to be:

$$R_2(SO_4)_3 \cdot (NH_4)_2SO_4 \cdot 8H_2O \rightarrow R_2(SO_4)_3 \cdot (NH_4)_2SO_4 \cdot 2H_2O + 6H_2O\uparrow, \quad (3)$$

$$R_2(SO_4)_3 \cdot (NH_4)_2SO_4 \cdot 2H_2O \rightarrow R_2(SO_4)_3 \cdot (NH_4)_2SO_4 \cdot H_2O + H_2O\uparrow, \quad (4)$$

$$R_2(SO_4)_3 \cdot (NH_4)_2SO_4 \cdot H_2O \rightarrow R_2(SO_4)_3 \cdot (NH_4)_2SO_4 + H_2O\uparrow. \quad (5)$$

Furthermore, a drastic weight loss suggesting the vaporization of $(NH_4)_2SO_4$ was observed around 400 °C for both groups (R=Pr, Nd and R=Sm, Eu solids). However, since exothermic peaks were observed in the temperature range of 300–320 °C, anhydrous $R_2(SO_4)_3 \cdot (NH_4)_2SO_4$ decomposes to $R_2(SO_4)_3$ and $(NH_4)_2SO_4$, as suggested by previous reports [9]. Therefore, $R_2(SO_4)_3 \cdot (NH_4)_2SO_4$ (R=Pr, Nd, Sm, Eu) solids should fully decompose at approximately 300 °C.

3.3. Infrared spectra of $R_2(SO_4)_3 \cdot (NH_4)_2SO_4 \cdot xH_2O$

To determine the temperature at which the crystallization water vaporizes completely, infrared measurements were taken for $R_2(SO_4)_3 \cdot (NH_4)_2SO_4 \cdot xH_2O$ (R=Pr, Nd, Sm, Eu) by heating the $R_2(SO_4)_3 \cdot (NH_4)_2SO_4 \cdot 8H_2O$ solids at 120–260 °C for 10 h. Fig. 3 shows IR spectra of $R_2(SO_4)_3 \cdot (NH_4)_2SO_4 \cdot xH_2O$ solids (R=Pr (a), Sm (b)). The typical absorption frequencies observed for $R_2(SO_4)_3 \cdot (NH_4)_2SO_4 \cdot 8H_2O$ salt are also tabulated in Table 3. For all solids, a sharp band at 1640 cm^{-1} for the H–O–H bend and an intense broad band extending from 3600 to 3000 cm^{-1} for the stretching mode of H_2O was clearly observed. Furthermore, the presence of R–OH_2 stretching (430 cm^{-1}) and R–$(OH)_2$ wagging (485 cm^{-1}) bands indicated that the water molecules were coordinated to the rare-earth ions (although these bands overlapped the ν_2 vibrations of the sulfate group (SO_4)).

When the sulfate group (SO_4) coordinates to another element in the structure, the high symmetry of SO_4 (T_d) should be lowered to C_{3v} (unidentate) or C_{2v} (bidentate or bridged). For $R_2(SO_4)_3 \cdot (NH_4)_2SO_4 \cdot 8H_2O$ salts, absorption bands were observed at 1200–1030 cm^{-1}, suggesting that a bridging bidentate sulfate group exists in the structure. Furthermore, the absence of the combination of asymmetric bending (ν_4) and intermolecular vibration (ν_6) bands (around 2000 cm^{-1}) for the ammonium ion indicates that the ammonium ion may have a free rotation in the structure [13,16]. Since all $R_2(SO_4)_3 \cdot (NH_4)_2SO_4 \cdot 8H_2O$ (R=Pr, Nd, Sm, Eu) solids had similar spectra based on the bands derived from the existence of H_2O, SO_4, NH_4, and the rare-earths, the IR results also indicate that all of the $R_2(SO_4)_3 \cdot (NH_4)_2SO_4 \cdot 8H_2O$ (R=Pr, Nd, Sm, Eu) solids had similar structure.

In the IR spectra of $Pr_2(SO_4)_3 \cdot (NH_4)_2SO_4 \cdot xH_2O$ solids, which were obtained by heating $Pr_2(SO_4)_3 \cdot (NH_4)_2SO_4 \cdot 8H_2O$ solid at 120–180 °C, the peaks derived from the bonds of H_2O (highlighted

Table 3
Infrared absorption frequencies in the 4000–400 cm^{-1} range for $R_2(SO_4)_3 \cdot (NH_4)_2SO_4 \cdot 8H_2O$ (R=Pr, Nd, Sm, Eu).

Assignment	Observed frequencies (cm^{-1})			
	Pr	Nd	Sm	Eu
ν (H_2O)	3510	3550	3505	3525
ν_3 (NH_4)	3252	3258	3263	3256
δ (H_2O)	1641	1677	1636	1637
ν_4 (NH_4)	1437	1437	1436	1435
ν_3 (SO_4)	1146	1154	1147	1146
	1112	1113	1116	1122
	1063	1069	1069	1072
ν_1 (SO_4)	988	990	991	992
ν_4 (SO_4)	650	652	653	653
	616	617	617	617
ν_2 (SO_4)+R–(OH) wagging	481	482	485	483
R–OH_2 stretch	430	429	436	431

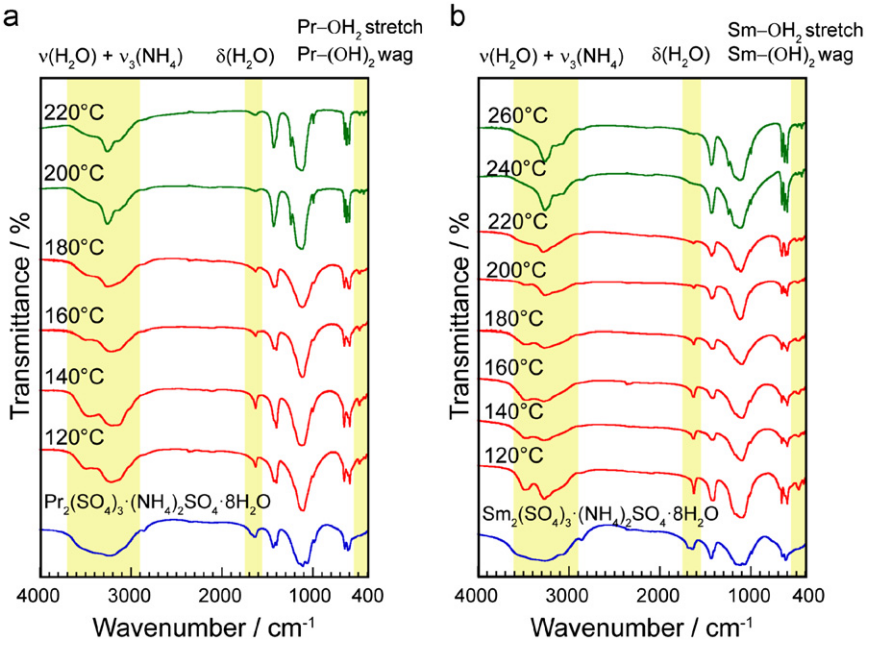

Fig. 3. IR measurement results of $R_2(SO_4)_3 \cdot (NH_4)_2SO_4 \cdot xH_2O$ obtained by heating $R_2(SO_4)_3 \cdot (NH_4)_2SO_4 \cdot 8H_2O$ solids at 120–260 °C for 10 h (R=Pr (a), R=Sm (b)). The IR spectra of $R_2(SO_4)_3 \cdot (NH_4)_2SO_4 \cdot 8H_2O$ is also depicted for comparison.

in Fig. 3) weakened with increasing temperature, suggesting the vaporization of crystallization water. Furthermore, no meaningful absorption bands implying the existence of H_2O were observed in samples heated above 200 °C, although the band observed around 3600–3000 cm^{-1} remained because the v_4 band of NH_4 exists around 3250 cm^{-1}. From these results, the temperature at which the crystallization water in the $Pr_2(SO_4)_3 \cdot (NH_4)_2SO_4 \cdot 8H_2O$ solid completely vaporizes was determined to be 180–200 °C, which corresponds well with the TG-DTA results. A quite similar dehydration behavior was also observed for $Nd_2(SO_4)_3 \cdot (NH_4)_2SO_4 \cdot xH_2O$.

Similarly, the temperature at which the crystallization water in $R_2(SO_4)_3 \cdot (NH_4)_2SO_4 \cdot 8H_2O$ (R=Sm, Eu) completely vaporizes was found to be 220–240 °C. In the TG-DTA results for the double salt of R=Sm, Eu (Fig. 1b), gradual weight loss suggesting the vaporization of one water molecule was observed between 145 and 240 °C. Since the IR results strongly support the TG-DTA data, the dehydration behavior of $R_2(SO_4)_3 \cdot (NH_4)_2SO_4$ (R=Sm, Eu) was also clarified.

3.4. Raman spectrometry of anhydrous $R_2(SO_4)_3 \cdot (NH_4)_2SO_4$

To determine the stable temperature region for anhydrous $R_2(SO_4)_3 \cdot (NH_4)_2SO_4$ double salt, Raman measurements were carried out for anhydrous $R_2(SO_4)_3 \cdot (NH_4)_2SO_4$ solids which were obtained by heating $R_2(SO_4)_3 \cdot (NH_4)_2SO_4 \cdot 8H_2O$ solids at 220–340 °C for 10 h. Fig. 4 shows the Raman spectra of anhydrous $R_2(SO_4)_3 \cdot (NH_4)_2SO_4$ solids (R=Pr (a), Sm (b)), with the corresponding spectra of $R_2(SO_4)_3 \cdot (NH_4)_2SO_4 \cdot 8H_2O$ and $R_2(SO_4)_3$. The Raman data and assignments for $(NH_4)_2SO_4 \cdot R_2(SO_4)_3$ (R=Pr, Nd, Sm, Eu) are given in Table 4. The normal vibrations of tetrahedral SO_4 should be observed at frequencies of 981, 451, 1104, and 613 cm^{-1} for v_1, v_2, v_3, and v_4 modes, respectively. For all $R_2(SO_4)_3 \cdot (NH_4)_2SO_4 \cdot 8H_2O$ double salts, Raman peaks derived from SO_4 bonds were confirmed, and included the bands of symmetric vibration of SO_4 (v_1) (965–1000 cm^{-1}), symmetric deformation vibration (v_2) (420–490 cm^{-1}), asymmetric stretch (v_3) (1100–1150 cm^{-1}), and asymmetric bending (v_4) (610–645 cm^{-1}). For $Pr_2(SO_4)_3 \cdot (NH_4)_2SO_4$ solid (Fig. 4a) heated at 220–260 °C, the S/N ratio of the spectra decreased with increasing temperature, and the intensity of the peak assigned to SO_4 decreased. Furthermore, Raman peaks derived from SO_4 in the double salt disappeared at 280 °C, indicating that the $Pr_2(SO_4)_3 \cdot (NH_4)_2SO_4$ had completely decomposed. Although the Raman spectra for the samples heated up to 280 °C are noisy, the sample completely decomposed to the $R_2(SO_4)_3$ has no meaningful noise in a spectrum. The reason why the spectra for the samples heated between 220 and 280 °C are noisy is considered to be due to the dehydration of the sample, suggesting the lower structural stability compared to the hydrated sample.

Similar behavior was observed for $Sm_2(SO_4)_3 \cdot (NH_4)_2SO_4$. Although bands suggesting the existence of SO_4 units in the anhydrous $Sm_2(SO_4)_3 \cdot (NH_4)_2SO_4$ were observed at 280–300 °C, bands assigned to $Sm_2(SO_4)_3$ appeared for the samples heated above 320 °C. The appearance of $Sm_2(SO_4)_3$ indicates that $Sm_2(SO_4)_3 \cdot (NH_4)_2SO_4$ decomposes to $Sm_2(SO_4)_3$ and $(NH_4)_2SO_4$. These Raman measurement results for $R_2(SO_4)_3 \cdot (NH_4)_2SO_4$ at elevated temperatures are well consistent with the gradual weight loss around 300 °C observed in the thermal analysis (Fig. 2).

Table 4
Raman spectral data and assignments for $R_2(SO_4)_3 \cdot (NH_4)_2SO_4 \cdot 8H_2O$ (R=Pr, Nd, Sm, Eu).

Assignment	Observed frequencies (cm^{-1})			
	Pr	Nd	Sm	Eu
v_2 (SO_4)	425 487	423 486	425 488	425 452
v_4 (SO_4)	619 633	612 635	618 640	615 642
v_1 (SO_4)	994	975 993	965 995	998 977
v_3 (SO_4)	1108 1150	1109	1114	1119

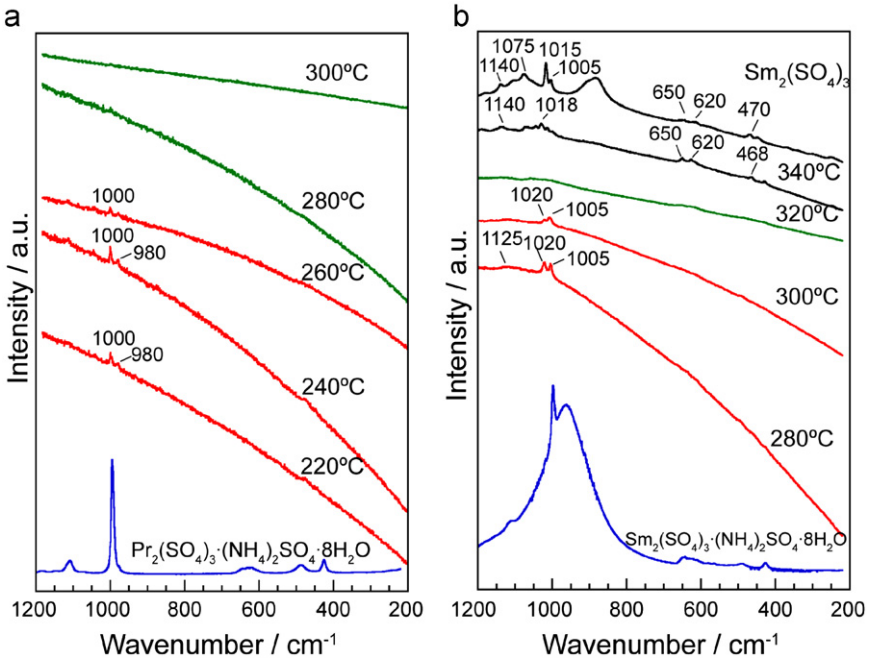

Fig. 4. Raman spectra of $R_2(SO_4)_3 \cdot (NH_4)_2SO_4$ obtained by heating $R_2(SO_4)_3 \cdot (NH_4)_2SO_4 \cdot 8H_2O$ solids at 220–340 °C for 10 h (R=Pr (a), R=Sm (b)). The Raman spectra of $R_2(SO_4)_3 \cdot (NH_4)_2SO_4 \cdot 8H_2O$ and $R_2(SO_4)_3$ are also presented for comparison.

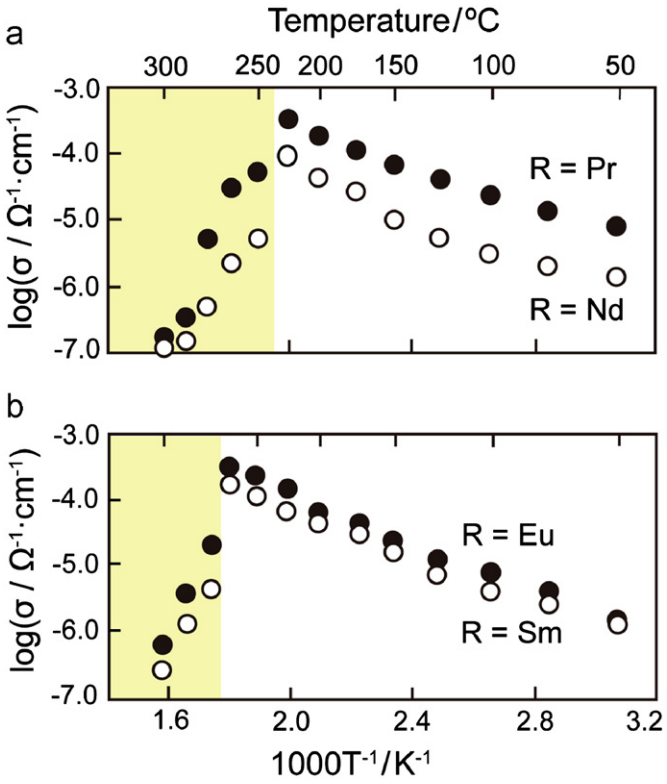

Fig. 5. Temperature dependences of the electrical conductivity for anhydrate $R_2(SO_4)_3 \cdot (NH_4)_2SO_4$ solids: (a) R=Pr, Nd and (b) R=Sm, Eu.

3.5. Electrical conductivity of rare-earth ammonium sulfate $R_2(SO_4)_3 \cdot (NH_4)_2SO_4$

Since the electrical conductivity of rare-earth ammonium sulfate should change with the decomposition of $R_2(SO_4)_3 \cdot (NH_4)_2SO_4$, we measured the electrical conductivities of anhydrous $R_2(SO_4)_3 \cdot (NH_4)_2SO_4$ (R; Pr, Nd, Sm, Eu) solids, which were obtained by heating $R_2(SO_4)_3 \cdot (NH_4)_2SO_4 \cdot 8H_2O$ solids at 200 °C (R=Pr, Nd) and 240 °C (R=Sm, Eu) for 10 h. Fig. 5 shows the temperature dependences of the electrical conductivity for the anhydrous $R_2(SO_4)_3 \cdot (NH_4)_2SO_4$ in the temperature range from 50 to 350 °C. For the R=Pr, Nd salt, the conductivity monotonically increased with increasing temperature up to 230 °C. However, the conductivity of the $R_2(SO_4)_3 \cdot (NH_4)_2SO_4$ solids decreased rapidly above 250 °C. Similarly, the conductivity of Sm, Eu salts also increases with increasing temperature, and then decreased above 300 °C. These results are consistent with the estimated temperature where $R_2(SO_4)_3 \cdot (NH_4)_2SO_4$ decomposes to $R_2(SO_4)_3$ and $(NH_4)_2SO_4$. Since the electrical conductivity change during heating reflects the thermal decomposition of the sample, the $R_2(SO_4)_3 \cdot (NH_4)_2SO_4$ solids may begin to decompose into $R_2(SO_4)_3$ and $(NH_4)_2SO_4$ at 250 and 300 °C for R=Pr, Nd and R=Sm, Eu, respectively.

The thermally stable temperature region for anhydrous $R_2(SO_4)_3 \cdot (NH_4)_2SO_4$ estimated from TG-DTA, IR, Raman, and electrical conductivity measurements are summarized in Fig. 6.

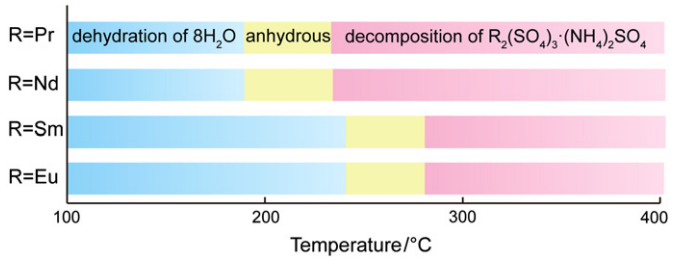

Fig. 6. Stable temperature region for anhydrous $R_2(SO_4)_3 \cdot (NH_4)_2SO_4$ (R=Rr, Nd, Sm, Eu).

The thermal stabilities of anhydrous $R_2(SO_4)_3 \cdot (NH_4)_2SO_4$ are quite different from those reported in the literature, which were obtained from only TG-DTA (Pr: 193–375 °C, Nd: 190–360 °C, Sm: 190–333 °C, Eu: 230–342 °C) [9].

4. Conclusions

We have clarified the stable temperature range of anhydrous rare-earth ammonium sulfate $R_2(SO_4)_3 \cdot (NH_4)_2SO_4$ double salts, which we expect to be utilized as a practical solid-state material. Among the series $R_2(SO_4)_3 \cdot (NH_4)_2SO_4$, the single phases of $R_2(SO_4)_3 \cdot (NH_4)_2SO_4$ were obtained for samples with R=Pr, Nd, Sm, and Eu. Detailed characterization of these double salts indicated that the thermal stability of anhydrous $R_2(SO_4)_3 \cdot (NH_4)_2SO_4$ is different between (Pr, Nd) and (Sm, Eu). Since the previous reports were based only on thermal analysis, the present work has more accurately determined the exact thermal stability of $R_2(SO_4)_3 \cdot (NH_4)_2SO_4$ solids.

Acknowledgment

This work has been supported in part by Grant-in-Aid for JSPS Fellows (No. 21671) from the Japan Society for the Promotion of Science.

References

[1] T. Sato, F. Ozawa, S. Ikoma, J. Appl. Chem. Biotechnol. 28 (1978) 811–822.
[2] J.P. Pizzolato, H.A. Papazian, J. Am. Ceram. Soc. 53 (1970) 289–290.
[3] H. Bassett, T.H. Goodwin, J. Chem. Soc. (1949) 2239–2279.
[4] L. Campbell, S. Debenedetti, Phys. Lett. 20 (1966) 103–105.
[5] V.M. Petrugevski, W.F. Sherman, J. Molec. Struct. 294 (1993) 171–176.
[6] B.V.R. Chowdaiu, J. Phys. Chem. Solids 30 (1969) 2747–2757.
[7] M.E. Garcia-Clavel, M.P. Servert-Buxados, Thermochim. Acta 144 (1989) 65–73.
[8] A.P. Belousova, I.V. Shakhno, V.E. Plyushchev, Russ. J. Inorg. Chem. 15 (1970) 116–120.
[9] L.D. Iskhakova, I.E. Sukhova, O.P. Chernova, I.V. Shakhno, V.E. Plyushchev, Russ. J. Inorg. Chem. 20 (1975) 193–196.
[10] E. Staritzky, D.T. Cromer, Anal. Chem. (1956) 554–555.
[11] P.N. Iyer, P.R. Natarajan, J. Less-Common Met. 146 (1989) 161–166.
[12] B. Erikson, L.O. Larsson, L. Ninisto, U. Skoglund, Inorg. Chem. 13 (1974) 290–295.
[13] P.N. Iyer, P.R. Natarajan, Thermochim. Acta 210 (1992) 185–192.
[14] T. Nagai, S. Tamura, N. Imanaka, Sens. Lett. 6 (2008) 454–457.
[15] T. Nagai, S. Tamura, N. Imanaka, ECS Trans. 16 (11) (2008) 257–264.
[16] C. Postmus, J.R. Ferraro, J. Chem. Phys. 48 (1967) 3605–3610.